Quantitative analysis of the Arabidopsis shoot apical meristem during floral transition

A thesis
Submitted towards the partial fullfilment of
BS-MS dual degree programme
by

John Thampi

Date: 10/04/2023

under the guidance of

Dr Pau Formosa-Jordan and Prof Dr George Coupland

Department of Plant Developmental Biology, Max Planck Institute for Plant Breeding Research, Cologne

from Jul 2022 to Apr 2023

Indian Institute of Science Education and Research Pune

Certificate

This is to certify that this dissertation entitled "Quantitative analysis of the Arabidopsis shoot apical meristem during floral transition" submitted towards the partial fulfillment of the BS-MS degree at the Indian Institute of Science Education and Research, Pune represents original research carried out by John Thampi at Max Planck Institute for Plant Breeding Research, Cologne, under the supervision of Dr Pau Formosa-Jordan and Prof Dr George Coupland during academic year July 2022 to April 2023.

Supervisor:
DR PAU FORMOSA-JORDAN
GROUP LEADER,
MAX PLANCK INSTITUTE FOR
PLANT BREEDING RESEARCH

Digitally signed by Pau Formosa Jordan
Date: 2023.05.22 08:43:01 +02'00'

Co - Supervisor:
PROF DR GEORGE COUPLAND
DIRECTOR,
MAX PLANCK INSTITUTE FOR
PLANT BREEDING RESEARCH

JOHN THAMPI
20181159
BS-MS
IISER PUNE

DATE: 10/04/2023

Declaration

I, hereby declare that the matter embodied in the report titled "Quantitative analysis of the Arabidopsis shoot apical meristem during floral transition" is the results of the investigations carried out by me at the Max Planck institute for Plant Breeding Research from the period 01/07/2022 to 31/03/2023 under the supervision of Dr Pau Formosa-Jordan and Prof Dr George Coupland and the same has not been submitted elsewhere for any other degree.

Supervisor:
DR PAU FORMOSA-JORDAN
GROUP LEADER,
MAX PLANCK INSTITUTE FOR
PLANT BREEDING RESEARCH

Co - Supervisor:
PROF DR GEORGE COUPLAND
DIRECTOR,
MAX PLANCK INSTITUTE FOR
PLANT BREEDING RESEARCH

JOHN THAMPI
20181159
BS-MS
IISER PUNE

DATE: 10/04/2023

Acknowledgements

I would like to express my heartfelt gratitude to my supervisor Dr Pau Formosa-Jordan for being an excellent guide and mentor. I would like to thank my supervisors Dr Pau Formosa-Jordan and Prof Dr George Coupland for their valuable comments and advice on the project.

I would like to thank my thesis expert Dr Kalika Prasad for his involvement in the project

I would also like to thank Dr Martina Cerise for providing all the experimental data used in this study and performing part of the image analysis.

I would like express my gratitude to Dr Athul Vijayan for all teaching me his nuclear segmentation pipeline and all the help he offered.

My fellow group members at the Formosa-Jordan group were most kind and helpful during my stay, and I would like to thank them.

This project would have not been possible without the support of the Max Planck Institute for Plant Breeding Research and IISER Pune.

Finally, I would like to thank all my friends and family for their love and support during this endeavour.

Contributions

Contributor name	Contributor role
John Thampi	Performed the research - methodology design, cell and nuclear segmentation, meristem morphology and data analysis, writing.
Martina Cerise	Image acquisition and cell segmentation
Athul Vijayan	Methodology - Nuclear segmentation
Gabriel Rodriguez Maroto	Methodology - Meristem morphology
Pau Casanova-Ferrer	Methodology - Meristem morphology
Mirjam Thielen	Cell segmentation
Pau Formosa Jordan	Designed and supervised the research. Feedback on the writing.
George Coupland	Designed and supervised the research

Abstract

The stem-cell niche at the Shoot Apical Meristem (SAM) in *Arabidopsis thaliana* undergoes reorganisation during floral transition. This niche is maintained by a well-studied negative feedback loop between *WUSCHEL* and *CLAVATA3*, but how this network evolves during floral transition is unknown. In this study, we use confocal imaging and a custom cellular-resolution quantitative image analysis pipeline to study the expression domains of these two genes in the SAM during the floral transition using transcriptional reporters of *WUSCHEL* and *CLAVATA3* in wild-type and two mutant lines. We provide a first description of their patterning during floral transition. We find a transient expansion in the expression domain of *WUSCHEL* - pointing to a role of the rib zone of the meristem in maintaining stem-cell homeostasis. Our work helps further the current understanding of stem-cell homeostasis in the shoot apical meristem, and of the organisation of the SAM in general. It provides a quantitative framework for future experimental and modelling studies of the system.

Contents

List of Figures

Chapter 1

Introduction

1.1 The cradle of organs - the Shoot Apical Meristem

Plants have the remarkable capacity to produce organs throughout their lifetime - giving rise to the wonderful diversity of form in the flora we see across the biosphere. This persistent organogenesis necessitates the maintenance of stem cells in the plant throughout its life cycle and requires the plant to have tight control over the processes of growth, molecular patterning, and cell-fate decision-making, regardless of its age or environmental conditions. The shoot apical meristem (SAM) and the root apical meristem (RAM) are the primary sites of organ generation in plants, established during embryogenesis (Bowman and Eshed, 2000)and harbour stem cells that produce all above- and below-ground organs, respectively. The SAM is particularly intriguing as it can produce organs of different identities depending on the stage of the plant's life cycle. It produces leaves during the vegetative phase and flowers during the reproductive phase. *Arabidopsis thaliana* is a particularly valuable system to study plant morphogenesis - since it is an extensively studied model system with well-characterised mutant lines

The shoot apical meristem in *Arabidopsis thaliana* is classified into different regions based on the arrangement of different cell types inside the tissue. The expression of *SHOOT MERISTEMLESS* (*STM*) - a homeodomain transcription factor - is usually used to define the meristematic region (Long *et al.*, 1996). Stem cells are located in an upward-facing cone-shaped region of reduced growth and division at the very tip of the meristem - called the central zone (CZ) (Fletcher *et al.*, 1999). Flanking the CZ on all sides is the peripheral zone (PZ) - the descendants of the stem cells in the CZ move into this region and differentiate (Barton, 2010); it is a region of extensive cell division - from which incipient organ primordia emerge - be it leaves or flowers. Cells at the apical tip of the CZ are organised into layers (Poethig, 1987) - called the L1, L2, and L3 (Lopes *et al.*, 2021) - due to the anticlinal division(perpendicular to the surface of the meristem) of stem cells in the CZ. Just below the CZ, with some overlap, is a group of cells called the organising centre (OC) (Mayer *et al.*, 1998). The cells in the OC are responsible for specifying and maintaining the stem-cell fate of cells in the CZ. The region below the OC is called the rib meristem - a site of un-oriented cell division.

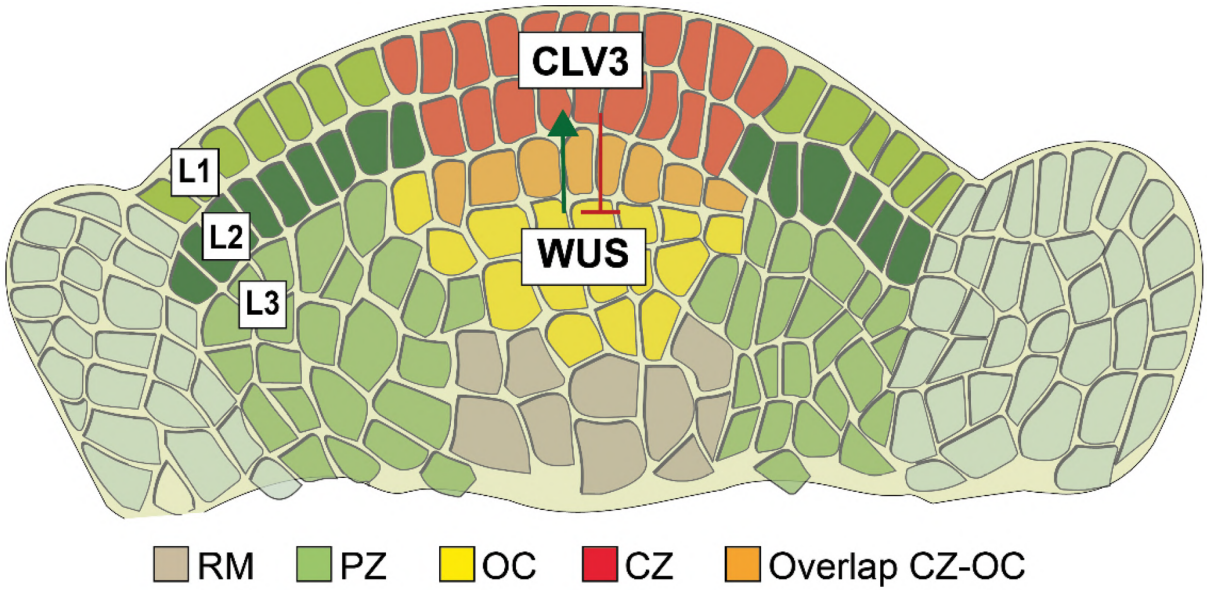

Figure 1.1: **Organization of the SAM.** The SAM in *Arabidopsis thaliana*is organised into zones. A negative feedback loop between *WUSCHEL* and *CLAVATA3* maintains stem-cell homeostasis. Adapted from (Lopes *et al.*, 2021).

1.2 Stem cell homeostasis in the SAM

1.2.1 The WUSCHEL-CLAVATA3 Feedback Loop

The stem cell niche in the Arabidopsis SAM is maintained by a well-studied transcriptional negative feedback loop between *WUSCHEL* and *CLAVATA3* (Brand *et al.*, 2000; Schoof *et al.*, 2000). *WUS* is expressed in the cells of the OC and encodes a diffusible homeodomain transcription factor that is responsible for the promotion of stem-cell fate (Mayer *et al.*, 1998) in the CZ through repression of the differentiation programme (Yadav *et al.*, 2011; Daum *et al.*, 2014). Loss-of-function *wus* mutants have been observed to produce defective meristems that terminate prematurely (Laux *et al.*, 1996). *WUS* moves into the CZ through plasmodesmata (Daum *et al.*, 2014) and activates the transcription of *CLAVATA3* - which encodes a small, diffusible peptide - by binding to its promoter (Yadav *et al.*, 2011). CLV3 is secreted into extracellular space (Brand *et al.*, 2002) and represses the transcription of *WUS* by binding to CLV1 receptor proteins (Clark *et al.*, 1993) at the cell surface. *CLV3* loss-of-function mutants exhibit larger meristems and more organs due to uninhibited *WUS* expression (Clark *et al.*, 1995; Fletcher *et al.*, 1999). This forms the basic structure of the negative feedback loop proposed to explain stem-cell homeostasis in the SAM. While informative, this simple model does not give much insight into the spatial organisation and confinement of *WUS* and *CLV3* in the SAM. Looking at the structure of the feedback loop, since *CLV3* represses the expression of *WUS*, one might find the existence of the region of overlap of *WUS* and *CLV3* expression where both are maximally expressed counter-intuitive. Recent studies have characterised this gene regulatory network further and given us a more nuanced understanding of its spatial behaviour.

Recent studies looking at the homo-dimerisation of WUS have found support for a model in which WUS monomers promote *CLV3* expression, while WUS homodimers

repress *CLV3* expression (Busch *et al.*, 2010; Daum *et al.*, 2014), taking into account the differential mobility of WUS monomers and dimers (Fuchs and Lohmann, 2020). Another set of studies (Zhou *et al.*, 2015, 2018) looking at the interaction of WUS with *HAIRY MERISTEM* (HAM) - a family of transcription factors expressed in the L3 layer - have established that *WUS* and *HAM* form heterodimers. They proposed a model (Zhou *et al.*, 2018) for the confinement of *CLV3* to the CZ in which WUS-HAM heterodimers prevent the expression of *CLV3* in the OC while the absence of HAM in the CZ prevents heterodimerisation and induces expression of *CLV3*. This model has been supported by experimental perturbations in which the *ham1.2.3* loss-of-function mutant showed *CLV3* expression in the OC (Zhou *et al.*, 2015), and by computational simulations (Zhou *et al.*, 2018; Gruel *et al.*, 2018) which were able to capture both normal and mutant behaviour. Another study (Su *et al.*, 2020) has shown that WUS interacts with STM to form a heterodimer, promoting stronger binding to the *CLV3* promoter. Thus, stem-cell homeostasis in the SAM is a complex and many-layered process, and its mechanistic understanding necessitates mathematical modelling.

1.2.2 Modelling the WUS-CLV3 Feedback Loop

Biological systems have long provided fertile soil for phenomenological mathematical models to inform and answer questions of growth, molecular patterning, and differentiation. Formulating phenomenological rules as mathematical models and performing computational simulations have borne considerable fruits in understanding developmental processes such as morphogenesis and cell-fate determination. The *WUS-CLV3* feedback loop has also been a receptacle for the sunshine of modellers' attention, in part due to the interesting process at hand and in part because of the apparent simplicity of the network motif. The first model of *WUS-CLV3* (Jönsson *et al.*, 2005) implemented just the core feedback loop (refer to Section 1.2.1) coupled with a reaction-diffusion system in a 2-dimensional lattice of cells and was able to recapitulate the expression domain of *WUS* in wild-type and physically ablated meristems. However, the model used was based on the existence of a *hitherto* unknown mechanism that formed a pattern in the meristem. Subsequent experimental studies elucidating additional players in the maintenance of the SAM have enabled the development of more informed and complicated models (Geier *et al.*, 2008; Hohm *et al.*, 2010; Yadav *et al.*, 2013), which employ more molecular players and additional interactions - such as cytokinins regulating *WUS* expression (Gruel *et al.*, 2018), and peripheral zone and L1 signalling (Gruel *et al.*, 2016, 2018).

While these modelling studies have provided mechanistic insights into the maintenance and spatial organisation of the *WUS* and *CLV3* expression domains, we do not possess information on how these domains evolve during the floral transition - which represents a significant amount of reorganisation within the meristem unfolding over quite a short amount of time.

1.3 The Floral Transition

Plants undergo several developmental transitions throughout their life, and the organs produced at the SAM have differing identities based on the stage of the plant's life-cycle. One developmental transition of particular importance is the floral transition - which marks the end of the vegetative phase and the beginning of the reproductive phase in

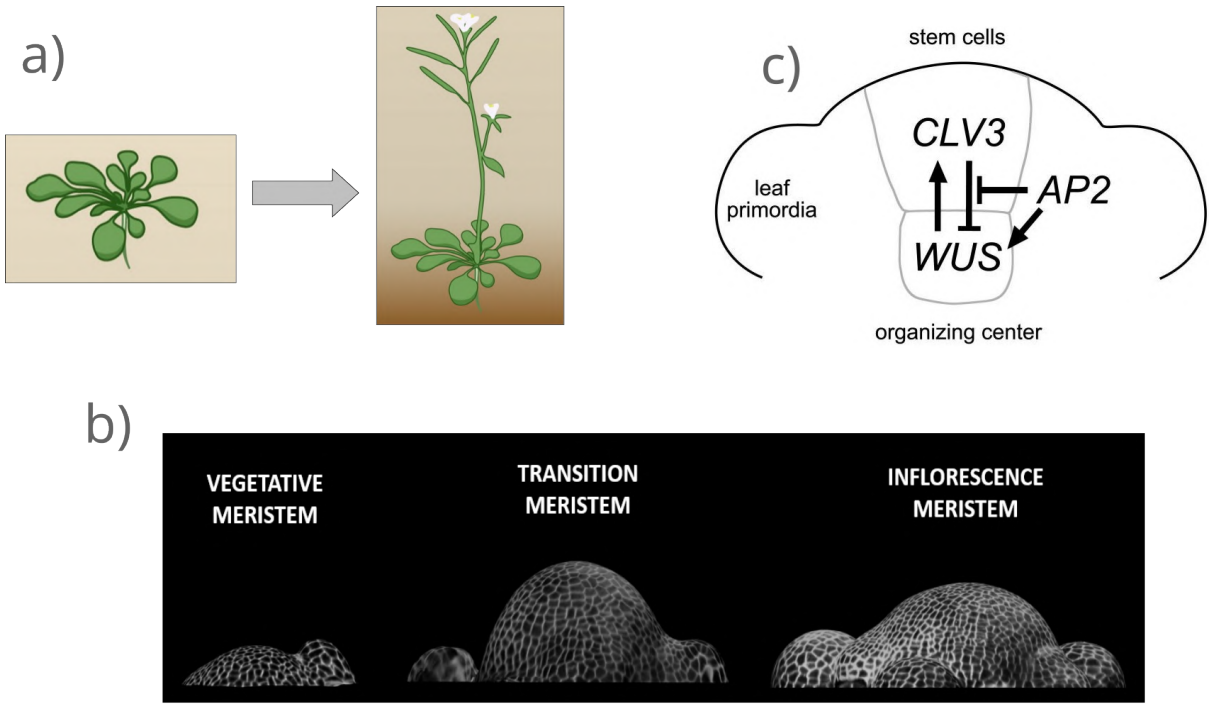

Figure 1.2: **The floral transition in *Arabidopsis thaliana*** a) The SAM shifts from producing leaves to producing flowers after the floral transition (Bäurle and Dean, 2006), b) The SAM undergoes morphological changes during floral transition(Images by Martina Cerise - unpublished) c) The hypothesised *WUS-CLV3* negative feedback loop with AP2 (Würschum *et al.*, 2006)

plants (Kinoshita *et al.*, 2020). The SAM goes from producing leaves during the vegetative phase, to producing flowers during the reproductive phase. This step is crucial in determining the survival of the plant and as such, depends on a complex gene regulatory network that integrates environmental signals such as photoperiod, age, sugar content, etc with hormonal signalling in the plant. A summary of the different pathways involved implicated in the floral transition can be found in (Conti, 2017). The floral transition is a period of pronounced morphological and physiological changes in the SAM. The vegetative meristem has a flat apical surface, but during the floral transition meristem, it adopts a distinct curved structure - in a process referred to as doming (Kinoshita *et al.*, 2020). The inflorescence meristem is also markedly larger in size than the vegetative meristem (Laufs *et al.*, 1998). The reason behind this coupling of the floral transition with doming is still not understood, and studying gene expression domains offers the exciting possibility of decoupling the same.

APETALA2 (*AP2*) is a transcription factor involved in multiple pathways that regulate flower and seed development (Okamuro *et al.*, 1997). In the floral transition, *AP2* is involved in the age-signalling pathway at the SAM. It acts a repressor of flowering, which is post-transcriptionally degraded by the microRNA172(miR172) - which accumulates as the plant ages (Ó'Maoiléidigh *et al.*, 2021). AP2 shows little expression in the floral meristem (Würschum *et al.*, 2006). *AP2* gain-of-function mutants are observed to be late-flowering, and *ap2* loss-of-function mutants are early-flowering. Our interest in *AP2* is due to the fact that it has been previously implicated in the *WUS-CLV3* feedback loop (Würschum *et al.*, 2006). *AP2* was proposed to promote WUS expression in the SAM;

and mutations in *AP2* have a similar effect to changes in *WUS* expression on the size of the SAM - with *AP2* gain-of-function mutants producing significantly larger SAMs. *AP2* thus provides us with a bridge between the stem-cell niche, meristem morphology, and the floral transition; and studying the evolution of *WUS* and *CLV3* expression domains in *AP2* gain- and loss-of-function mutants will allow us to study the effect of *AP2* on the WUS and CLV3 expression domains to better characterise its function in stem-cell homeostasis.

1.4 Motivations of the study

A common theme in studying the *WUS-CLV3* feedback loop in many of the studies mentioned above is the combined use of experimental perturbations and computational modelling. Studying a biological system such as the SAM - which undergoes significant morphological changes - requires researchers to obtain high resolution, time-lapse imaging data, perform quantitative analysis of these data, perform computational simulations to validate hypotheses and/or provide predictions to test out experimentally - which would feedback into this process. This synergistic framework - called computational morphodynamics (Formosa-Jordan *et al.*, 2022) - offers the possibility to efficiently leverage the developments in each of its constituent fields to in order to answer the biological question at hand.

Despite the presence of substantial research in understanding the *WUS-CLV3* system, the establishment and maintenance of their expression patterns in the meristem are not well understood. Using the approach of computational morphodynamics, we aim to study the evolution of the domains of expression of *WUS* and *CLV3* during the floral transition. We develop a high-throughput, quantitative image analysis pipeline to study the spatio-temporal evolution of *WUSCHEL* and *CLAVATA3*. Studying the proposed system requires us to have cellular resolution data on *WUS* and *CLV3* gene expression patterns. We use fluorescent transcriptional markers for both *WUS* and *CLV3* to visualise their domains of expression.

1.5 Aims of the study

This study aims to create a quantitative description of the shoot apical meristem in *Arabidopsis thaliana* during floral transition using the framework of computational morphodynamics. This includes:

1. Establishing a cellular resolution quantitative image analysis pipeline with the following capacity :
    (a) Perform accurate 3D segmentation of cell walls and nuclei in the SAM from confocal microscopy images of fluorescent marker lines.
    (b) Define domains of expression of transcription factors and calculate their effective concentrations
    (c) Extract geometrical features of expression domains and study their evolution
2. To create a quantitative description of the SAM during floral transition. This involves studying :

(a) Change in meristem morphology during floral transition using a pre-existing MATLAB code (RegionsAnalysis.

(b) Changes in the spatial organisation of *WUS* and *CLV3* expression domains to establish new observables indicating floral transition.

(c) The relation between meristem morphology and expression domains of *WUS* and *CLV3* in order to study their coupling

(d) The aforementioned properties in the rAP2 and *ap2_12* mutant lines in order to describe expression domains under flowering-time and size variations.

Chapter 2

Materials and Methods

2.1 Marker lines and Imaging

2.1.1 Plant growth conditions and genotypes

The lines *Arabidopsis thaliana* ecotype Columbia-0 wildtype, pAP2::rAP2 B2-1 mutants (Sang *et al.*, 2022) , and *ap2_12* (Yant *et al.*, 2010) mutants were used in in this study. All lines contained transcriptional fusions of pWUS::NLS-Venus and pCLV3::NLS-mCherry (Pfeiffer *et al.*, 2016), which in the *ap2_12* and pAP2::rAP2 B2-1 mutants were crossed by Dr Martina Cerise. The fluorescent proteins (Venus and mCherry) are targeted to the nucleus by a nuclear localisation signal in these lines. The rAP2 line encodes a version of the AP2 protein that is resistant to degradation by microRNA 172 (miR172). miR172 is increasingly expressed with age - hence rAP2 mutants have greater amounts of AP2 than the wild type at later stages of their life-cycle. The plants were grown under long-day conditions - 16 hours of light and 8 hours of darkness at 18-22°C - and their meristems were harvested at 7, 10, 13, 16, and 20 days of growth after seeding.

2.1.2 Sample preparation and confocal microscopy

Meristems of 7 seedlings at 7, 10, 13, 16, and 20 days after seeding were dissected under a stereoscopic microscope and leaves covering the SAM were carefully removed. Harvested SAMs were vacuumed twice and fixed in 4% paraformaldehyde maintained at 4°C for 2-3 days, after which they were washed with 1xPBS twice and fixed with 1.5mL ClearSee. The meristems were then treated with 1uL Renaissance solution 2 days prior to imaging. Four SAMs from each of the aforementioned time-points were imaged by Dr Martina Cerise and Mirjam Thielen using the Stellaris - 5 confocal microscope.

2.2 Image Processing

2.2.1 Cell segmentation

The acquired images underwent a preprocessing step in which the organ primordia were removed using the "Pixel Edit" tool in MorphoGraphX. The Renaissance channel staining the cell walls were segmented using the GASP (Bailoni *et al.*, 2022) algorithm in PlantSeg (Wolny *et al.*, 2020) after generating cell boundary predictions using the model "confocal_unet_bce_dice_ds3x" (Remadevi Vijayan, 2022). The segmentations were

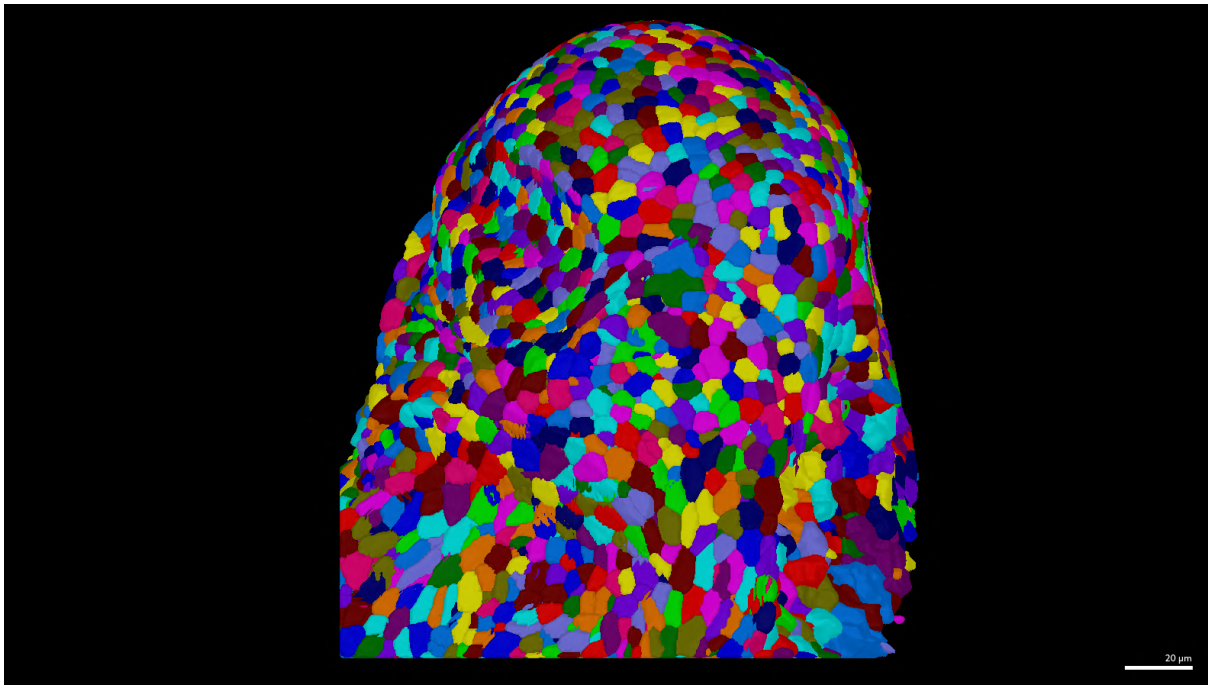

Figure 2.1: Cell walls segmented using PlantSeg - visualised in MorphoGraphX. Colours are used to visualise different cells separately. Scale bars are 20 μm.

manually corrected in MorphoGraphX. The segmented masks were converted to meshes and their features were quantified using the Heatmap process in MGX.

2.2.2 Nuclear segmentation

The Venus and mCherry channels from each image were merged using the maximal intensity at each pixel to segment the maximum number of nuclei - since we did not have a constitutively expressed nuclear marker. Predictions for nuclear boundaries were generated using the "confocal_unet_nuclei_stain_ds1x" model in PlantSeg. These predictions were imported into CellPose (Stringer *et al.*, 2021) and segmented using the model "nuclei" trained by Dr Athul Vijayan. The segmented masks were then scaled and reoriented using a Python script.

2.2.3 Connecting Cells to Nuclei

Since cell walls and nuclei were segmented separately, we matched segmented cells to segmented nuclei. A nucleus was paired to a cell if its centroid lay inside the cell. Conflicts arising due to one nucleus being split between 2 cells were resolved by pairing the nucleus with the cell that housed more than 50% of its volume. This was implemented using the "LineageTracking/Label nuclei" process in MGX.

2.2.4 Coordinate system

A cylindrical coordinate system centred at the apex of the meristem was defined to describe the spatial organisation of the meristem due to its radial symmetry. The origin of the coordinate system was manually placed at the apex of the meristem for each image

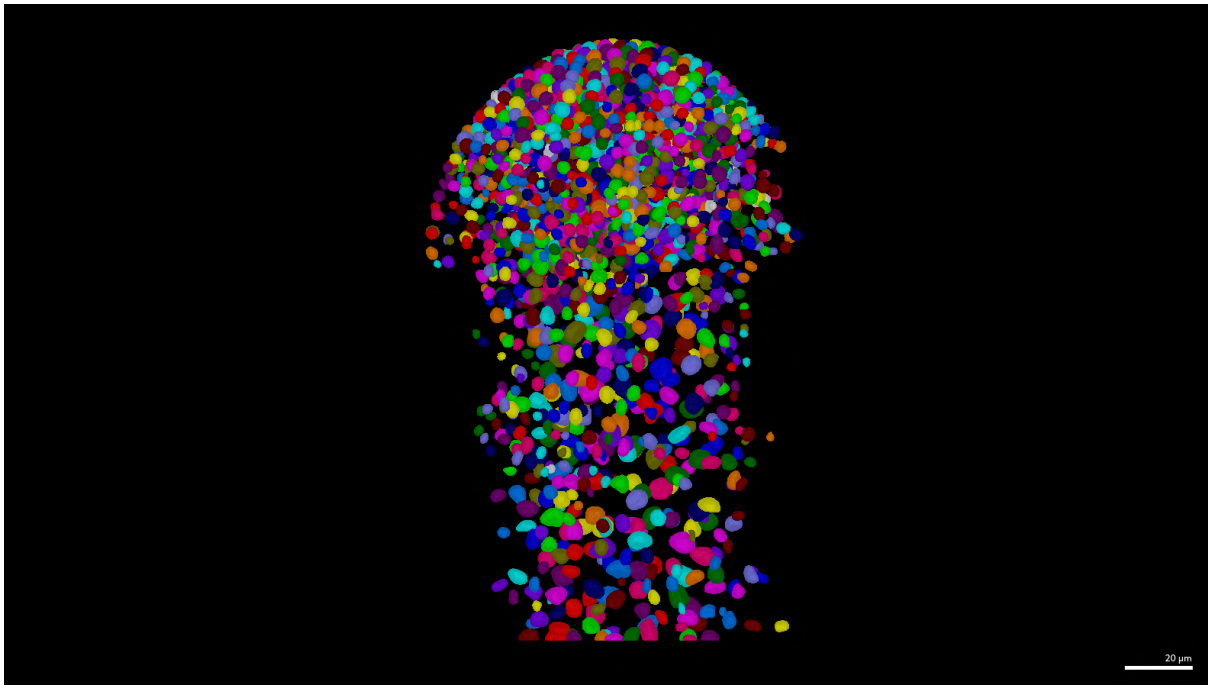

Figure 2.2: Nuclei segmented using PlantSeg and CellPose - visualised in MorphoGraphX. Colours are used to visualise different nuclei separately. Scale bars are 20 μm.

in MGX. The meristem was then aligned with the axes to reduce any tilt during imaging. The coordinates of the centroids of each cell and nucleus were then extracted using the Heatmap process in MGX. The coordinate transforms were carried out in Python.

2.2.5 Concentration definitions

The average signal intensity of inside a segmented nucleus was defined as the concentration of a transcription factor inside the nucleus. We assumed that the fluorescence intensity inside each nucleus is directly proportional to concentrations of the mRNA of the corresponding transcription factor. A second definition of concentration - given by the average signal intensity inside each segmented cell was also used. The choice between normalising signal intensity by nuclear size and normalising by cellular size was made by studying the relationship between the two. It was observed that cell size grew non-linearly with nuclear size, especially as one moved into the rib meristem. We also reasoned that nuclear concentrations would be the more relevant observable for defining the activity of transcription factors - since they act inside the nucleus.

2.3 Domains of expression

2.3.1 Thresholding

Since we were interested in describing how the activity of transcription factors changed spatially during the floral transition, we defined domains of expression for each transcription factor. In each image, cells with concentration greater than MAX/K were defined to be part of the domain of expression, MAX is the median of the 20 highest concentrations of a transcription factor in each meristem. This procedure was used to account for the

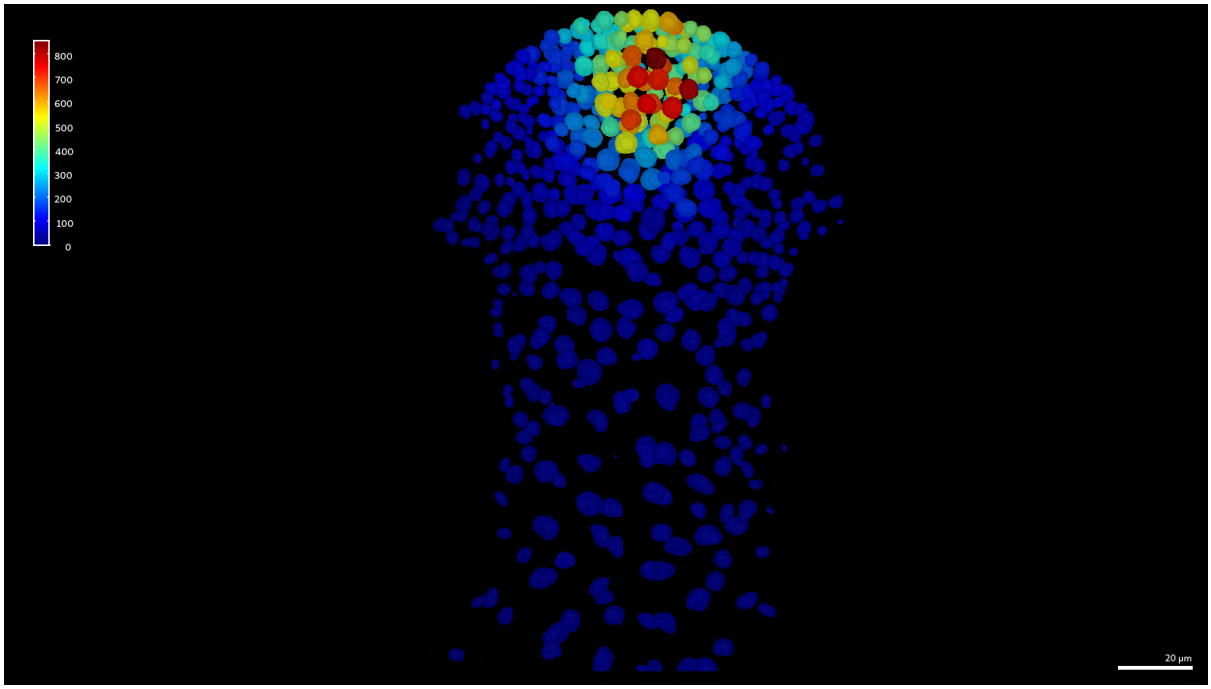

Figure 2.3: Nuclei coloured with *CLV3* concentrations - visualised in MorphoGraphX. Scale bars are 20 μm.

fact that normalisation across time points and genotypes could not be performed due to the absence of a constitutively expressed nuclear marker. Different values of K were tested and K = 5 was chosen for simplicity. It is important here to note that while we define discrete, bounded domains of expression, these boundaries do not necessarily exist - due to the graded nature of the domain. The "positive" nuclei for each transcription factor are to be taken as nuclei expressing the particular transcription factor strongly, as opposed to being the only nuclei affected by its activity. The consisting set of points consisting of the centroids of "positive" nuclei for each transcription factor were then clustered using DBSCAN - a density based clustering algorithm (see below for further details).

2.3.2 Clustering Expression Domains

After applying the aforementioned thresholding method, we applied the clustering algorithm DBSCAN (Ester *et al.*, 1996) (Density Based Spatial Clustering of Applications with Noise) to the 3D coordinates of each nucleus above the threshold, in order to exclude nuclei which were spaced far from the bulk of the domain of expression. The algorithm adds a point to a cluster if there are k points within a distance of e units. The parameter k was manually set to 5. e was calculated separately for each image by plotting nearest neighbour distances for all pairs of nuclei and selecting the value at which the distance increases sharply.

2.3.3 Domain features

The following metrics were used to describe the domains of expression of *WUS* and *CLV3*

1. **Number of cells/nuclei in the domain :** The number of nuclei in the clustered

domain were counted

2. **Volume of the domain :** the volume of an expression domain was calculated using two definitions
   (a) the sum of the volumes of all the cells in a domain calculated from the segmentation
   (b) the volume of the convex hull formed by the centroids of all nuclei in a domain. This was calculated using the ConvexHull function from the scipy.spatial Python Library.
3. **Width of the domain :** to calculate the width of an expression domain, the centroids of all cells in the domain were projected onto the yz-plane, and the boundary of the projection (obtained from a convex hull) was fit to an ellipse using a least squares fitting.
4. **Length of the domain :** the length of a domain was calculated as the distance between the apical and basal tip of the domain.

2.4 Meristem Morphology

Morphological features of the meristem such as curvature, height, and width were quantified using a custom made semi-automatic pipeline, using RegionsAnalyisis Matlab code. The pipeline involved taking two orthogonal projections of the membrane channel of each meristem, manually drawing a parabola between the youngest two primordia, and performing a least squares fitting of this curve to obtain height, width, and curvature as shown in Figure 2.4.

2.5 Statisical Testing

Tukey's Honest Significant Difference test was used to compare the a metric across each pair of timepoints. A *p-value* of 0.05 was used as threshold to determine if the difference between two groups was significant. All tests were performed using the Python module scipy.stats.

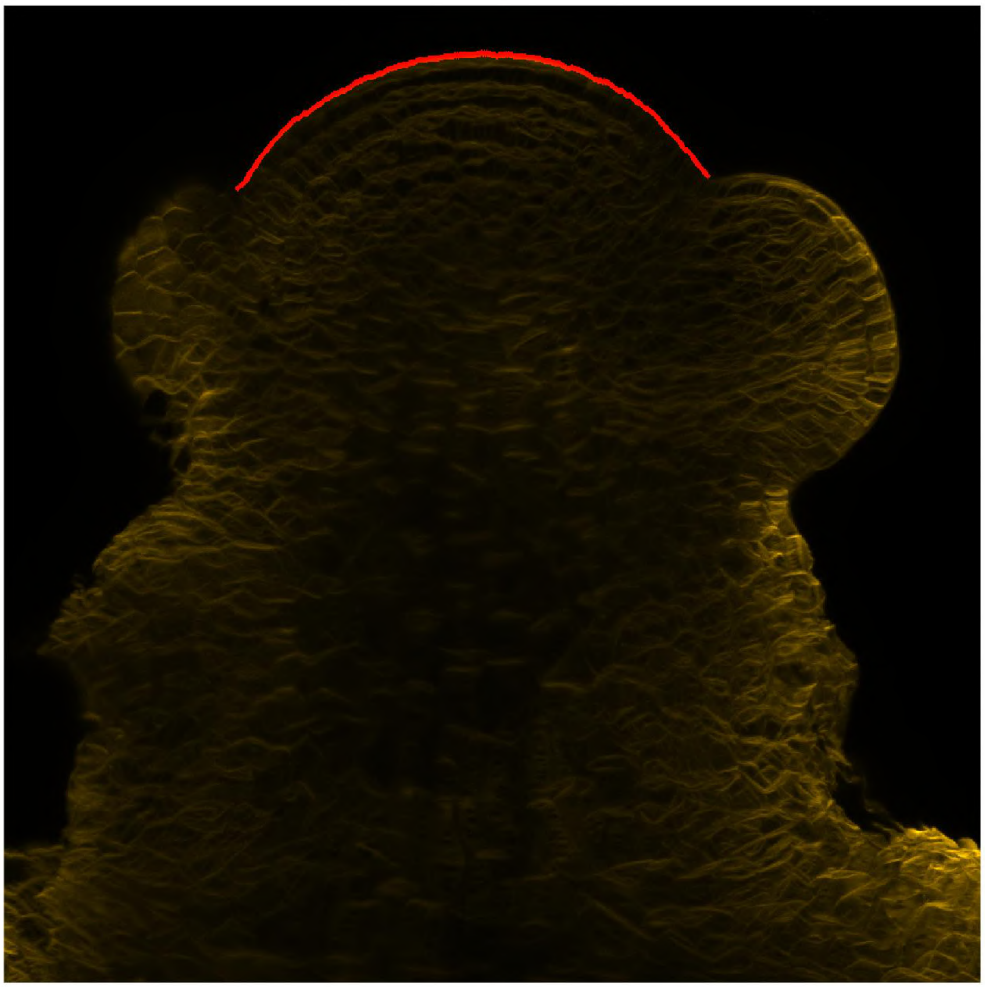

Figure 2.4: Maximal intensity projections on the xz and yz plane are used to draw and fit parabolas to the meristem and calculate morphological features using the RegionsAnalysis MATLAB code.

Chapter 3

Results

3.1 Quantitative characterisation of the wild type shoot apical meristem during floral transition

First, we established a quantitative description of the SAM in wild type Col-0 during floral transition, taking into account morphological features and gene expression patterns of *WUS* and *CLV3*. The following features were observed.

3.1.1 The shoot apical meristem undergoes doming during the floral transition

Morphological changes accompanying the floral transition were quantified by measuring the height, width, and curvature of the meristem along a time course using a pipeline from the MATLAB RegionsAnalysis code.

We observed that meristem height and curvature increased from 7 LDs to 13 LDs - where they reached their maxima, and then decreased until the last time point (Figure 3.1.1 f, g). Meristem width (Figure 3.1.1 h) shows a similar trend, peaking at 16 LDs. We reason from these observations that the doming phase characteristic of the floral transition takes place around 13 days after germination in inductive long day conditions. This exercise allowed us to characterise the meristem at 13 LDs as the transition meristem, and use it as a temporal reference to study gene expression patterns of *WUS* and *CLV3*.

3.1.2 WUSCHEL domain transiently expands into the rib meristem during floral transition

After defining the cells in the *WUSCHEL* expression domain (see Materials and Methods), we quantified the changes in *WUS* domain size and morphology during the floral transition. We observed an increase in the number of cells in the expression domain from 7 LDs to 13 LDs - with the peak corresponding to the previously determined timing of floral transition, and a subsequent decrease until the last time point. The size of the *WUS* domain was also quantified as the volume of the cells occupying the domain to get an idea of the means of domain expansion (cell division versus cell expansion). *WUS* domain volume showed the same trend as number of cells.

To explore the direction of *WUS* domain expansion, we measured the distance of the apical and basal tip of the *WUS* domain from the apex of the SAM. We observed

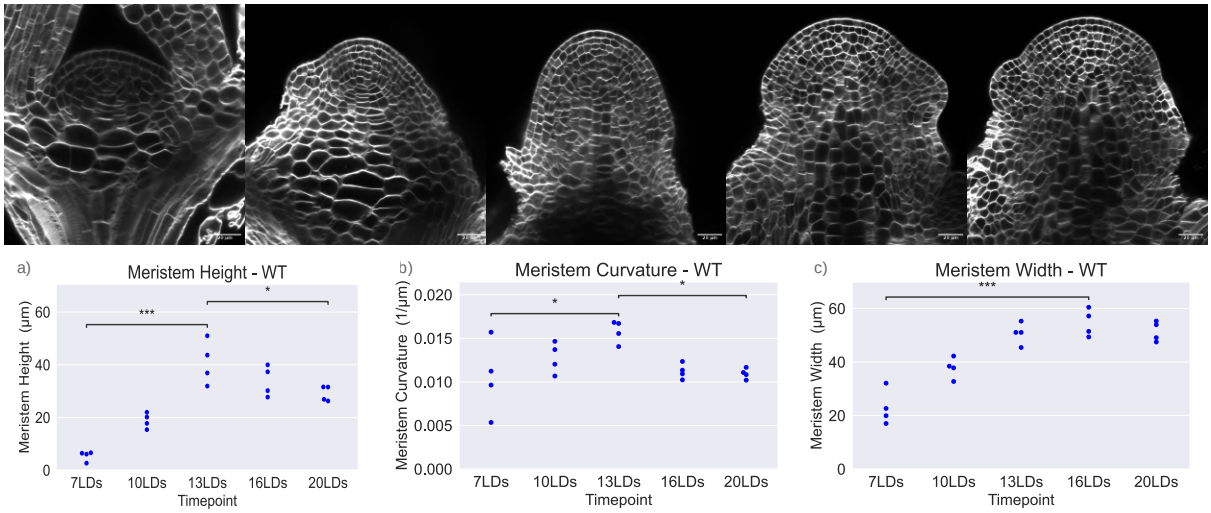

Figure 3.1: **The SAM undergoes doming during floral transition**. **(Top Row)** Maximal intensity projections of Col-0 SAM at 7, 10, 13, 16, and 20 long days after germination **(a, b)**. The SAM reaches peak height and curvature at 13 LDs **(c)** The width of the meristem peaks at 16 LDs. Scale bar represents 20 μm. Each time point has 4 datapoints. Asterisks denote p-values for Tukey's HSD test. * - $0.01<p<0.05$, ** - $p<0.01$, *** $p<0.001$, ns - $p>0.05$

that the *WUS* domain expanded into the rib meristem during floral transition, attaining maximum length at 13 LDs - exactly at the peak of the transition. We also observed a significant decrease in the width of the *WUS* domain from 13 LDs to 20 LDs. Domain length and width did not show significant correlation, and plotting the ratio of domain length to width showed that the there was a greater increase in length of the domain than in the. From these data, we established the behaviour of the *WUS* domain in wild-type and inferred that it transiently elongates into the rib meristem during floral transition.

3.1.3 *CLV3* domain expands during floral transition

The same procedure described above to characterise the *WUS* domain was used to study the evolution of the *CLV3* domain. We observed an increase in the number of nuclei expressing *CLV3* from 7 LDs to 16 LDs - where it peaked, and this trend was confirmed by domain volumes. The basal tip of the *CLV3* domain was observed to expand into the organising centre, with maximum penetration at 16 LDs. The width of the *CLV3* domain showed the same trend as the length. The length and width of the domain were strongly correlated, and the ratio of length to width did not vary much compared to the *WUS* domain's behaviour - showing a more symmetric increase in domain size. From these observations, we concluded that the *CLV3* domain expands during the floral transition. The peak of *CLV3* domain size falls one time-point after the *WUS* domain peaks - in line with the classical negative feedback-loop model in which *WUS* expression activates *CLV3* expression, and *CLV3* downregulates *WUS* expression. The lag between the *WUS* and *CLV3* expression maxima can be attributed to the time delay between *WUS* transcription, and subsequent translation and movement.

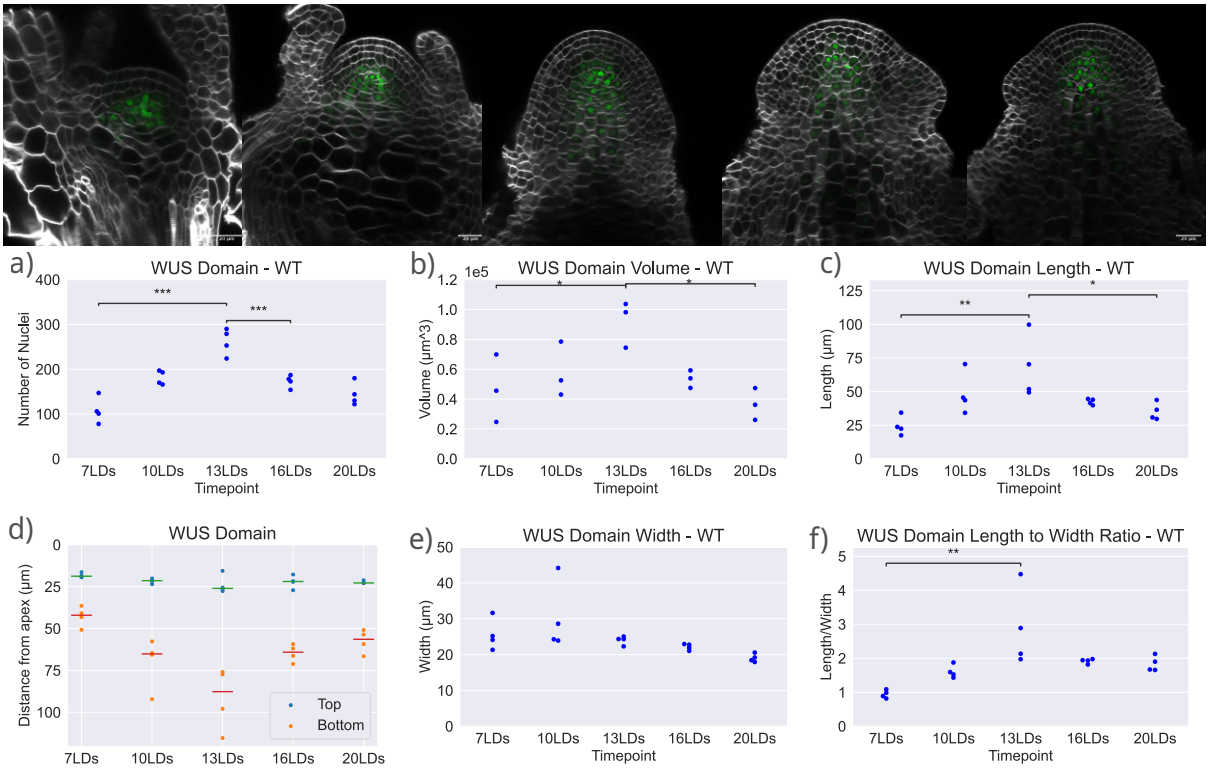

Figure 3.2: ***WUS* domain undergoes transient expansion during the floral transition.(Top Row)**Maximal intensity projections of Venus channel of Col-0 SAM at 7, 10, 13, 16, and 20 long days after germination. **(a)** The number of cells in the *WUS* domain, its **(b)** volume, **(c)** and length reach their peaks at 13 LDs and then reduce**(d)** The basal tip of the *WUS* domain (bottom) extends into the rib zone. **(e)** Width of the *WUS* domain. The basal tip of the *WUS* domain (bottom) extends into the rib zone. **(f)** Ratio of domain length to width shows the same trend as size of the domain. Scale bar represents 20 μm. Each time point has 3-4 data points. Asterisks denote p-values for Tukey's HSD test. * - 0.01<p<0.05, ** - p<0.01, *** p<0.001, ns - p>0.05

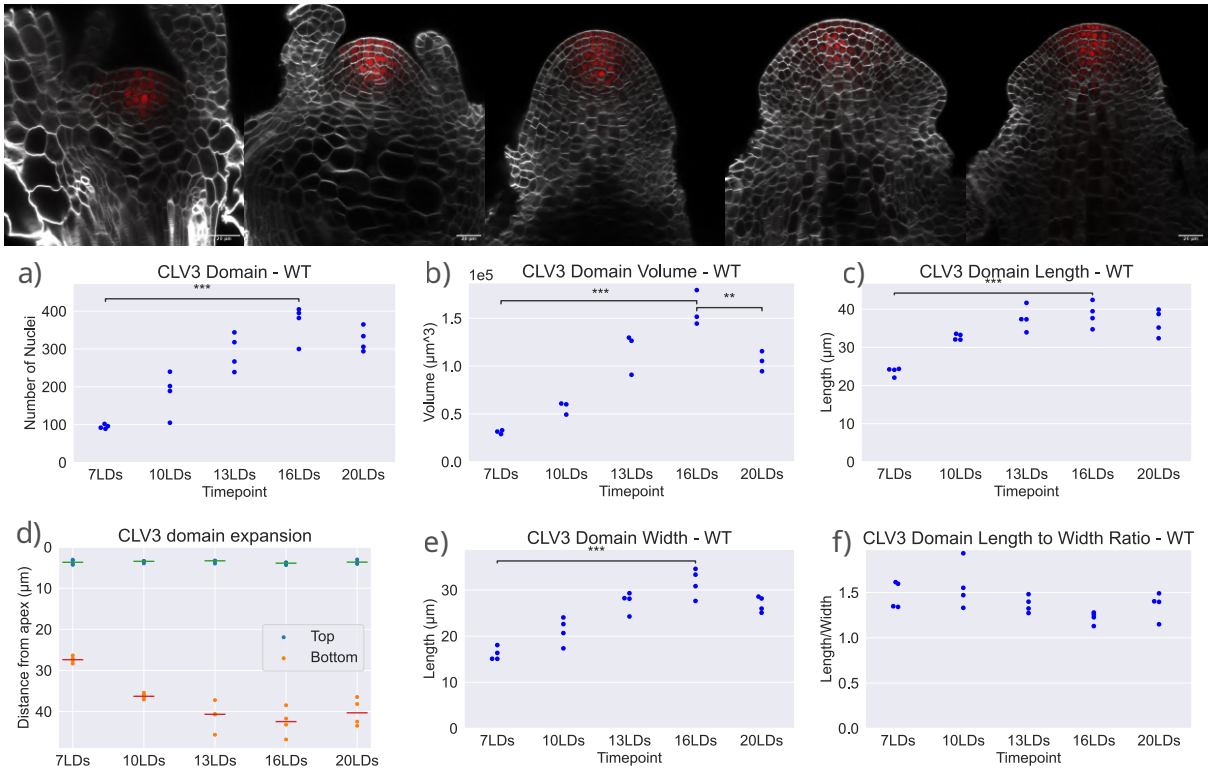

Figure 3.3: ***CLV3* domain expands during the floral transition**. **(Top Row)** Maximal intensity projections of mCherry channel of Col-0 SAM at 7, 10, 13, 16, and 20 long days after germination **(a)** The number of cells in the *CLV3* domain, **(b)** its volume, **(c)** length, and **(e)** width reach their peaks at 16 LDs **(d)** *CLV3* domain expands further into the *WUS* domain during floral transition. **(f)** Ratio of domain length to width. Scale bar represents 20 μm. Each time point has 3-4 data points. Asterisks denote p-values for Tukey's HSD test. * - 0.01<p<0.05, ** - p<0.01, *** p<0.001, ns - p>0.05

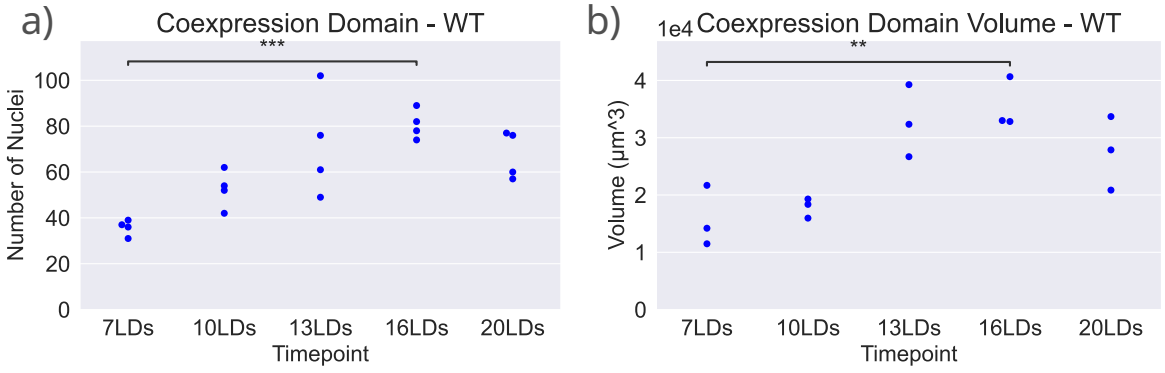

Figure 3.4: **Co-expression domain of *WUS* and *CLV3* expands during the floral transition**. **(a)** Number of cells expressing both *WUS* and *CLV3*. **(b)** Volume of the domain of co-expression of *WUS* and *CLV3*. Scale bar represents 20 μm. Each time point has 3-4 data points. Asterisks denote p-values for Tukey's HSD test. * - 0.01<p<0.05, ** - p<0.01, *** p<0.001, ns - p>0.05

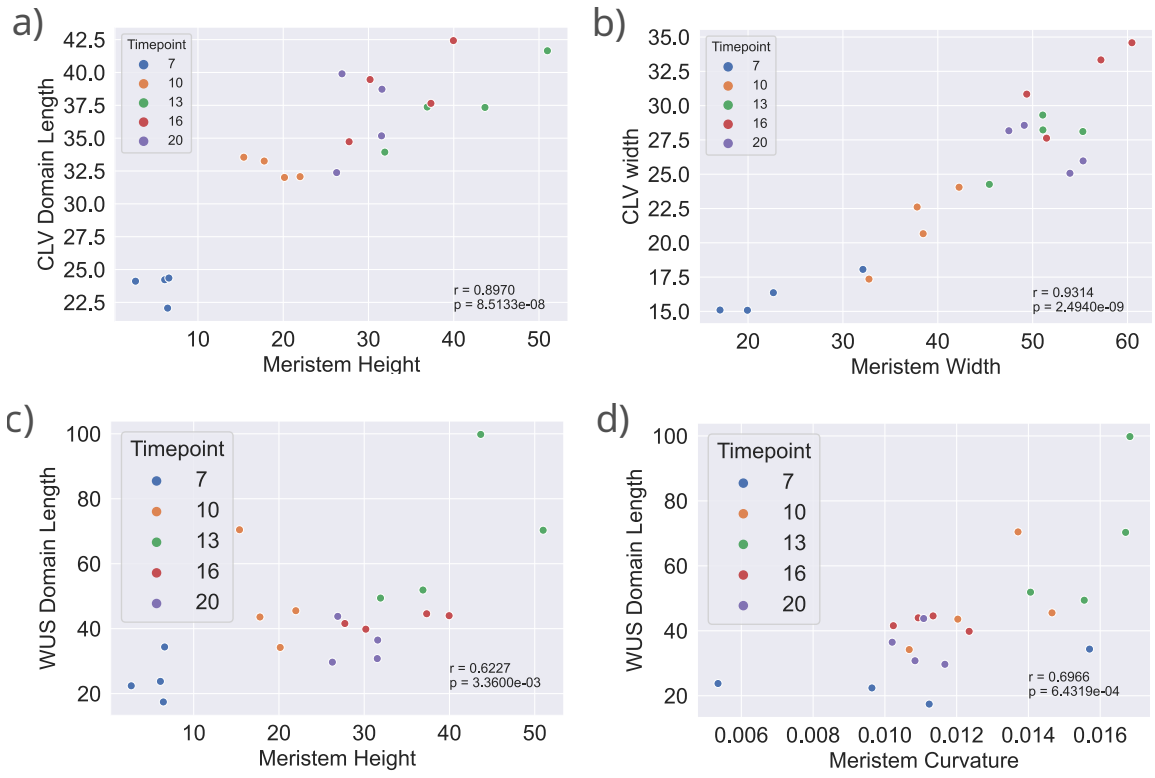

Figure 3.5: **Expression domains scale with meristem size**. **(a,b)** Length and width of the *CLV3* domain are correlated with height and width of the meristem.**(c, d)** Length of the *WUS* domain scales both with meristem length and curvature. r is the pearson correlation coefficient and p is the corresponding p-value. Each time point has 3-4 data points.

3.1.4 The coexpression domain of *WUS* and *CLV3* transiently expands during floral transition

The number of cells in the region that expressed both *WUS* and *CLV3* was observed to expand from 7 LDs to a maximum at 16 LDs. The length of the domain showed a similar trend as well. As the apical tip of the *WUS* domain does not move significantly during floral transition, we reasoned that this expansion of the overlapping zone was due to the *CLV3* domain extending into the OC.

3.1.5 Expression domains scale with meristem size

We studied the correlation between domain features and meristem morphology to see how expression domains scaled with meristem size. We observed that both the length and width of the *CLV3* domain were strongly correlated with the height and width of the meristem. This scaling was not observed in case of the width of the *WUS* domain, but domain height was observed to be correlated with meristem curvature and height.
In summary, we were able to create a quantitative description of the morphology and gene expression patterns in the wild-type SAM during floral transition. Next, to study how SAM morphology evolves during the floral transition in mutants with morphological defects, we described the SAM in *AP2* gain- and loss-of-function mutants using the same metrics.

3.2 Characterisation of *AP2* mutants during floral transition

3.2.1 *AP2* mutants show size defects

We characterised the morphology of the rAP2 and *ap2_12* mutant lines. The rAP2 line is a gain-of-function mutant in which AP2 is not degraded by miRNA172. We observed that the rAP2 line showed at least equal or greater meristem size than the wild type at all time points observed - as shown by the trends in meristem height and width (Figure 3.6 a,b). The evolution of these features showed the same temporal pattern as the wildtype (Figure 3.6 a-c).

In the *ap2* loss-of-function mutant, we observed that the meristems were of the same size or smaller than the wild-type at all time points - as seen by the trends in height (Figure 3.6d). We also observed that the curvature, height and width of the meristem peaked earlier in the *ap2_12* line - at 10 LDs, as opposed to 13 LDs in the wildtype. This behaviour is consistent with the early-flowering phenotype shown by *ap2* loss-of-function mutants

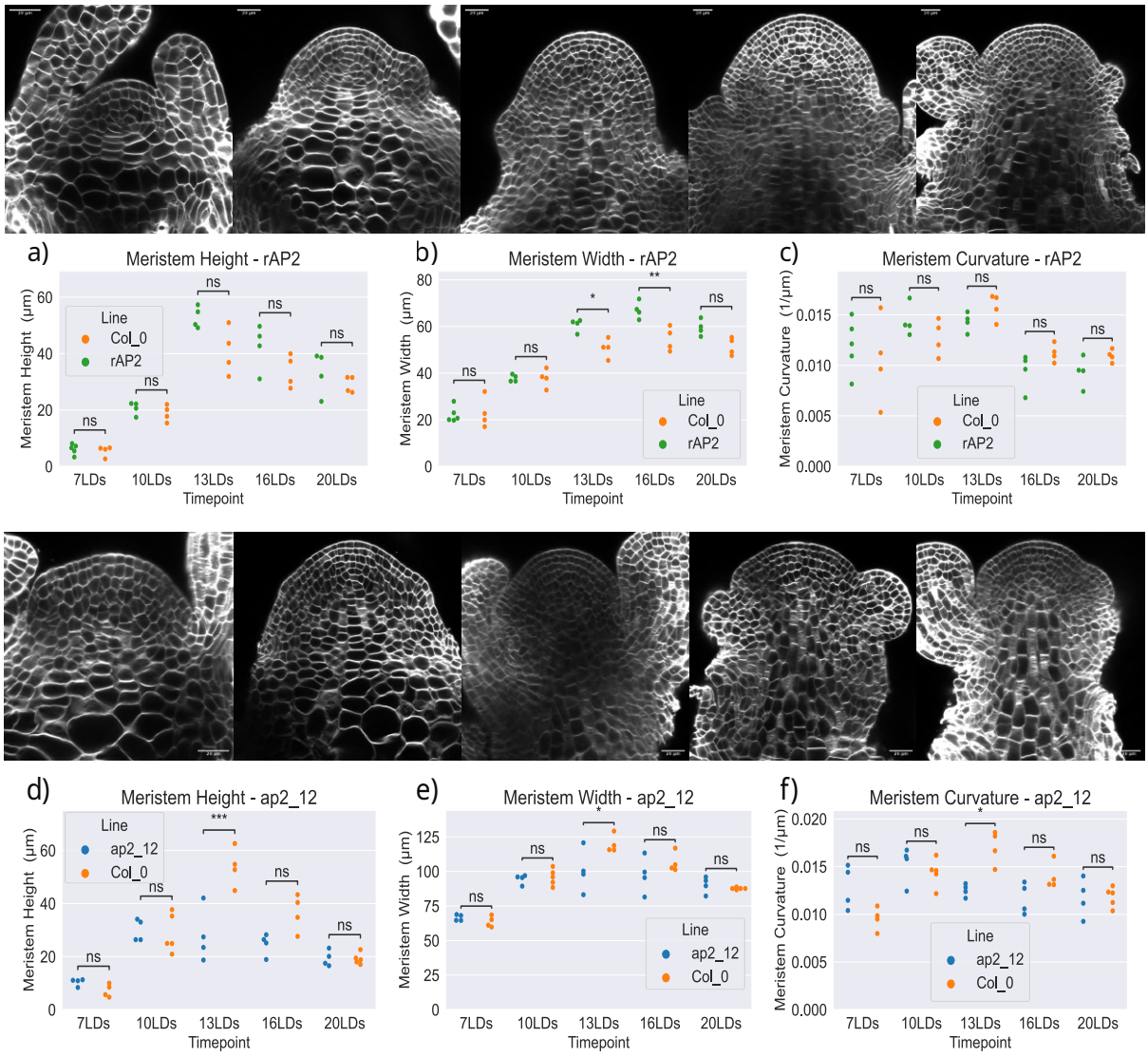

Figure 3.6: ***AP2* mutants show size defects.** Maximal intensity projections of the **(Top Row)** rAP2 and **(Middle Row)** *ap2_12* SAM at 7, 10, 13, 16, and 20 long days after germination. Height, width, and curvature of the SAM at 7, 10, 13, 16, and 20 long days after germination in the rAP2 **(a-c)** and *ap2_12* mutant**(d-f)** lines. Meristem size peaks at 10 LDs in the *ap2_12* line. Each time point has 4 samples.Scale bar represents 20 μm. Asterisks denote p-values for Tukey's HSD test. * - $0.01<p<0.05$, ** - $p<0.01$, *** $p<0.001$, ns - $p>0.05$

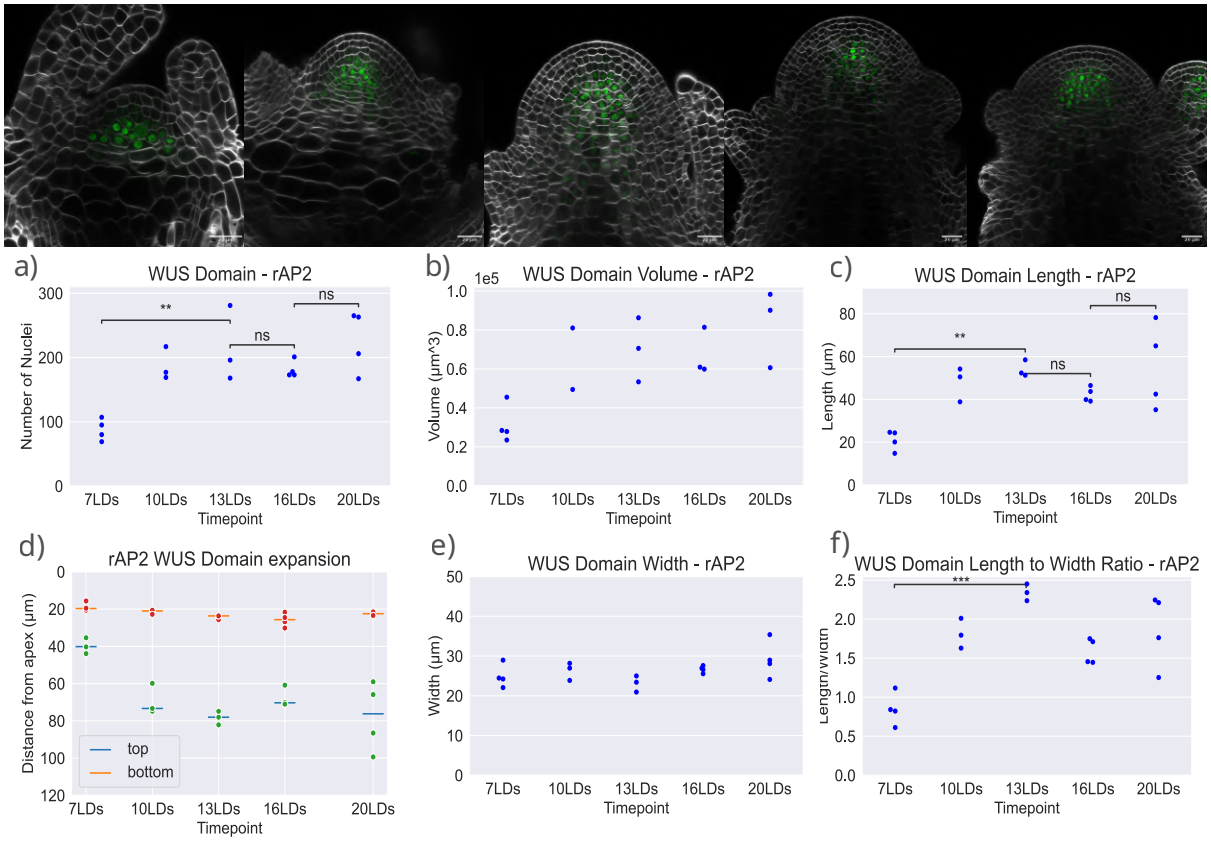

Figure 3.7: **Sustained expansion of the *WUS* domain in rAP2 mutants. (Top Row)**Maximal intensity projections of Venus channel of Col-0 SAM at 7, 10, 13, 16, and 20 long days after germination. (**a,b**) Expansion of the *WUS* domain can be seen from the trends in number of cells in the domain and volume. (**c, d**) Length of the *WUS* domain shows the same trend.**(e)** width of the *WUS* domain does not decrease as in *wild-type* **(f)** Ratio of domain length to width. Each time point has 3-4 samples. Scale bar represents 20 μm. Asterisks denote p-values for Tukey's HSD test. * - $0.01<p<0.05$, ** - $p<0.01$, *** $p<0.001$, ns - $p>0.05$

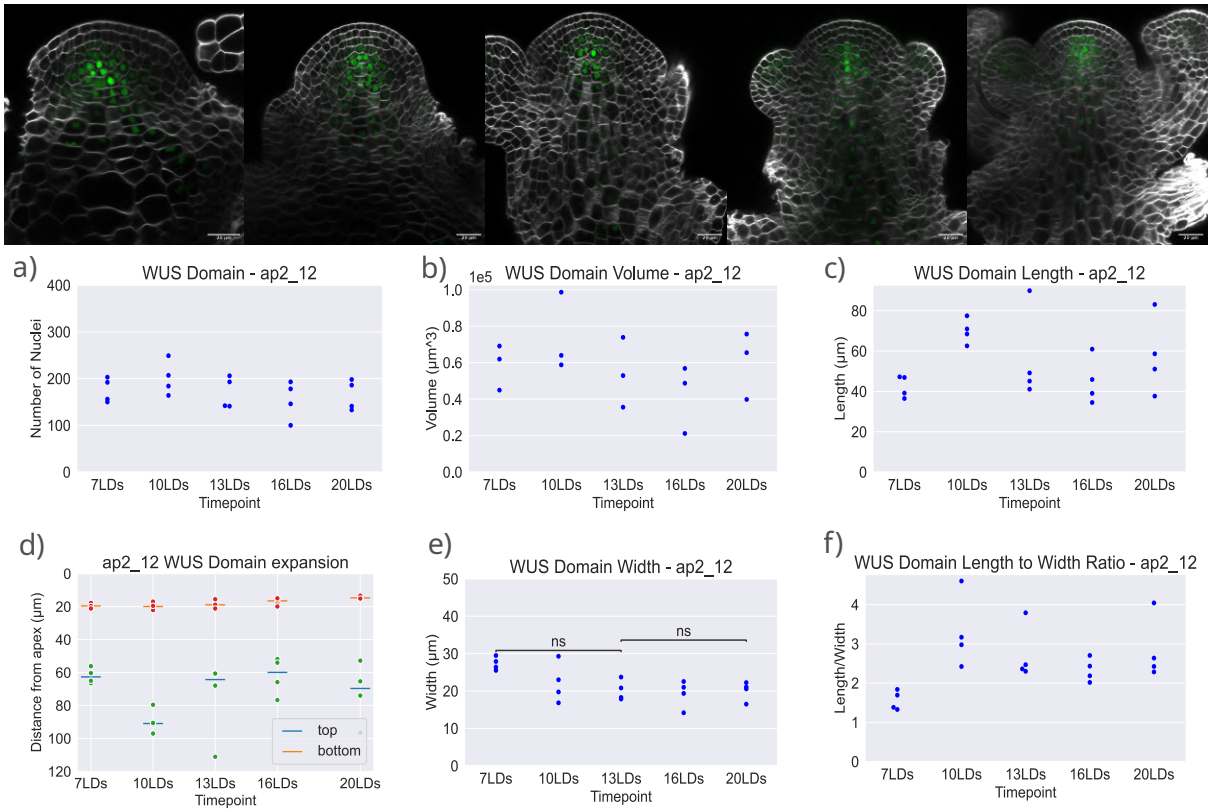

Figure 3.8: ***WUS* domain expands earlier in *ap2_12*. (Top Row)**Maximal intensity projections of Venus channel of Col-0 SAM at 7, 10, 13, 16, and 20 long days after germination. (**a,b**) Number of nuclei and volume of cells in the domain do not show significant changes. (**c, d**) Length of the *WUS* domain peaks at 13 LDs. **(e)** Width of the *WUS* domain decreases as in *wild-type*. **(f)** Ratio of domain length to width. Each time point has 3-4 samples. Scale bar represents 20 μm. Asterisks denote p-values for Tukey's HSD test. * - 0.01<p<0.05, ** - p<0.01, *** p<0.001, ns - p>0.05

3.2.2 WUS domain shows sustained expansion in the rib meristem in the rAP2 mutant

We quantified the size of the *WUS* domain in the rAP2 mutant as we had done with the wild-type and observed that there was a similar expansion of the domain from 7 LDs to 13 LDs - seen through both the number of cells and volume of the domain (Figure 3.7a,b). However, while the domain shrank in wild-type (Figure 3.2) after from 13 LDs to 20 LDs, this was not observed in rAP2 - which showed sustained *WUS* domain size through these time points. The same trend was observed in domain length as well (Figure c,d). Also in contrast to the wild-type, the *WUS* domain expanded in the horizontal direction from 13 LDs to 20 LDs (Figure 3.7 e). The ratio of domain length to width showed the same trend as the wild-type.The sustained expansion of the *WUS* domain is consistent with the hypothesised stem cell homeostasis network shown in Figure 1.2c. Absence of AP2 degradation by miR172 results in continued activation of *WUS*.

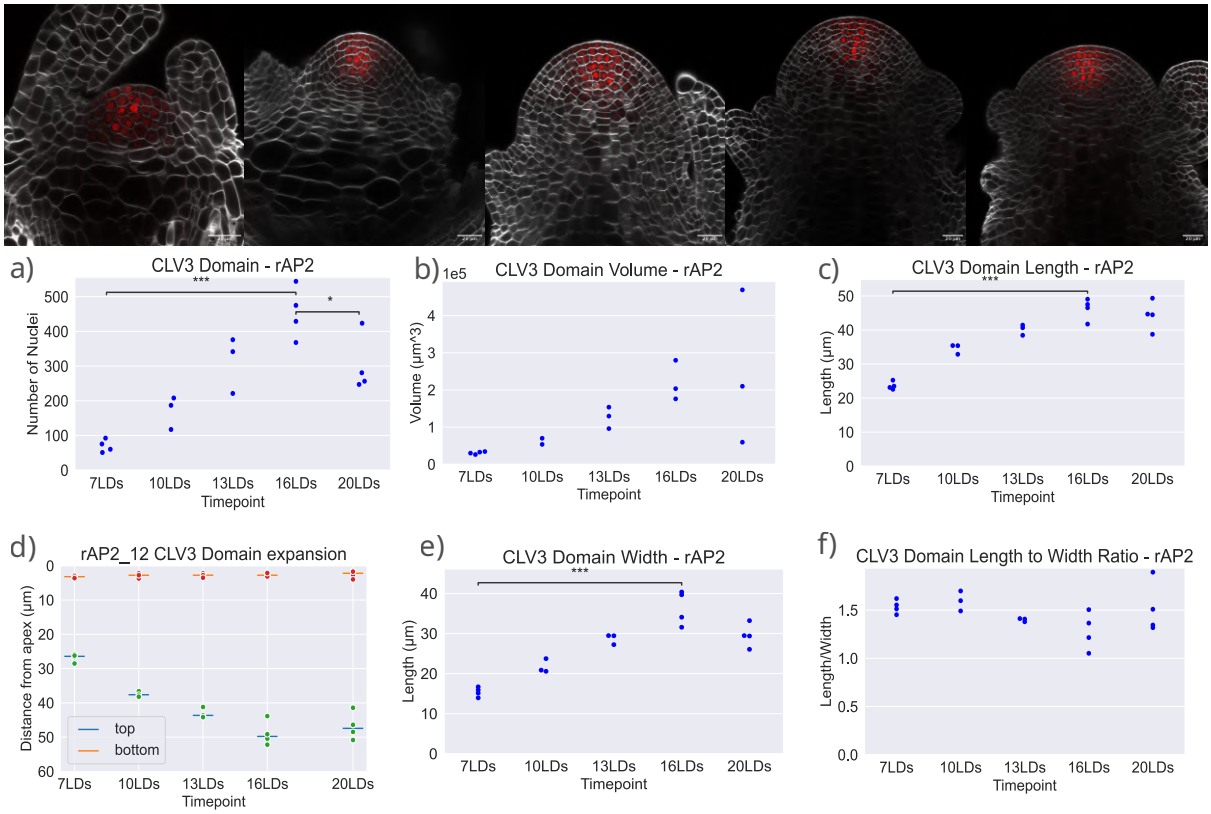

Figure 3.9: **rAP2 *CLV3* domains show the same behaviour as *wild-type*. (Top Row)** Maximal intensity projections of mCherry channel of Col-0 SAM at 7, 10, 13, 16, and 20 long days after germination. (**(a)**) Number of cells (**b**) Volume of *CLV3* domain. **(c, d)** Length of the *CLV3* domain. **(e)** Width of the *CLV3* domain **(f)** Ratio of domain length to width. Each time point has 3-4 samples. Scale bar represents 20 μm. Asterisks denote p-values for Tukey's HSD test. * - 0.01<p<0.05, ** - p<0.01, *** p<0.001, ns - p>0.05

3.2.3 The *WUS* domain expands earlier in the *ap2_12* mutant

In the *ap2_12* mutant we observed that there was no significant expansion in the number or volume of the *WUS* domain along the time course (Figure 3.8a,b). However, we observed an increase in the domain length from 7 LDs to 10 LDs (Figure 3.8c,d), showing an expansion of the domain into the rib meristem at an earlier stage than the wild-type (Figure 3.2). We did not observe significant changes in domain width (Figure 3.8e). The ratio of domain length to width behaved increased from 7 LDs to 10 LDs (Figure 3.8f), and did not change significantly until the last time point. From these observations, we concluded that the *WUS* domain of the *ap2_12* mutant line expands into the rib meristem earlier than in the wild-type - consistent with the early-flowering phenotype of *ap2* loss-of-function mutants.

3.2.4 *AP2* mutants show *CLV3* expression patterns similar to wild-type

CLAVATA3 domains in the rAP2 (Figure 3.9) and *ap2_12* (Figure 3.10) do not show significant differences from the wild-type (Figure 3.3) in any of the measured domain

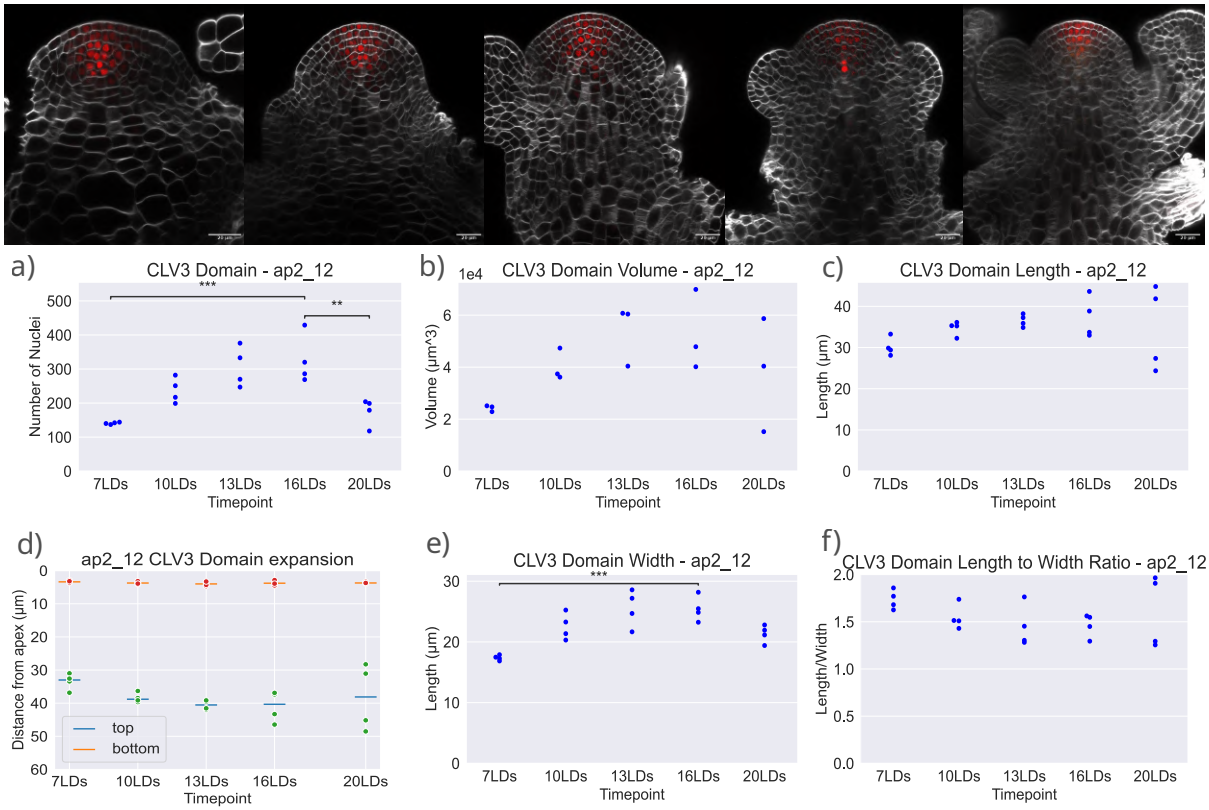

Figure 3.10: ***ap2_12 CLV3* domains show the same behaviour as *wild-type* (Top Row)** Maximal intensity projections of mCherry channel of Col-0 SAM at 7, 10, 13, 16, and 20 long days after germination. **(a)** Number of cells (**b**) Volume of *CLV3* domain. **(c, d)** Length of the *CLV3* domain. **(e)** Width of the *CLV3* domain **(f)** Ratio of domain length to width. Each time point has 3-4 samples. Asterisks denote p-values for Tukey's HSD test. * - 0.01<p<0.05, ** - p<0.01, *** p<0.001, ns - p>0.05

features. There was an increase in domain size from 7 LDs to 16 LDs in all lines studied.

Chapter 4

Conclusions and Discussion

4.1 Summary of main results from the study

4.1.1 A cellular resolution image analysis pipeline to study plant morphogenesis

Plant development involves a plethora of complex morphogenetic processes that require precise spatio-temporal regulation of gene expression and morphological change. These patterns are informed by genetics, environmental cues, and cell-cell communication. Any study of a developmental process hence requires precise spatio-temporal descriptions of the system of study. The development of advanced cellular resolution imaging techniques along with advanced 3D image analysis pipelines has provided us with the means to create such quantitative descriptions. In this study, we evaluated the performance of different deep-learning-based image segmentation protocols in performing accurate 3D segmentation of nuclei in the SAM from confocal images of fluorescent marker lines of *Arabidopsis thaliana*. We picked an image segmentation pipeline, optimised it for our data, and created a semi-automatic fluorescence quantification pipeline which can capture the spatial distribution of the concentration of transcription factors inside nuclei. We then used this pipeline to create a quantitative description of the shoot apical meristem during floral transition.

4.1.2 Organisation of the SAM during floral transition

We analysed morphological features of the shoot apical meristem and gained a quantitative understanding of how the shoot apical meristem changed shape during the floral transition. From our analysis of the wild-type Col-0, we established a timeline for the floral transition (in this particular line, under the conditions described in Section 2.1) allowing us to characterise it as the transition meristem - the intermediary between vegetative and inflorescence states. Using this timeline, we were able to use transcriptional marker lines for WUSCHEL and CLAVATA3 to study how the expression of these key players in stem-cell homeostasis evolved spatio-temporally during floral transition. We saw that the SAM underwent dynamic reorganisation during floral transition and observed a previously undocumented expansion of the WUS expression domain into the rib zone in the transition meristem. We then analysed the SAM of mutant lines. We observed that this elongation was sustained in the rAP2 mutant line untill our last timepoint of observation - consistent with the late-flowering phenotype shown by the line.

The WUS domain in *ap2_12* mutants expanded into the rib meristem earlier than in the wild-type, consistent with its early-flowering phenotype. Our observations in the mutant lines confirm the phenomenon that we observed in the wild-type and its link to the floral transition.Our results support the hypothesis that AP2 promotes WUS expression. However, the other hypothesised interaction - AP2 inhibiting CLV3's repression of WUS, remains to be tested. Vaidating or falsifying the model further motivates mathematical modelling of the system.

4.2 Discussion

The shoot apical meristem is the birthplace of all above-ground organs and represents an important system for the study of stem-cell homeostasis. However, though it is widely studied, we still lack a precise understanding about how the regions such as the rib meristem are organised, and how it changes during the floral transition. Our understanding of the SAM grows less and less clear as we move down from the L1 layer into the rib zone, which represents the least characterised region of the meristem. It remains shrouded in mystery, and its definitions vary depending on what one reads. One reason for the same is a lack of organisation in the region - which makes it difficult to study, compared to systems like the root apical meristem - which has a distinct organisation. This study highlights the importance of the rib zone in the context of stem-cell homeostasis. The WUSCHEL CLAVATA3 feedback loop is a well-studied system in the field of plant development, but its dynamic behaviour during development remains to be studied. We took first steps in this direction by studying the spatial behaviour of WUS and CLV3 expression during the floral transition.

Our study identified a novel feature in the SAM - that the domain of expression of WUS expands into the rib zone. This expansion could be due to several mechanisms. The SAM undergoes doming during floral transition and there is considerable cell expansion and division during this process. The cells in the WUS domain divide along the apico-basal axis of the meristem() and this could lead to an expansion of cells exhibiting WUS expression. This expansion of the WUS domain points to a role for the gene in the organisation of the rib zone. The scaling behaviour of CLV3 domains to meristem size suggests the possibility of adaptive scaling of the domain to tissue size, as seen for WUS in (Gruel *et al.*, 2016). We do not observe the same scaling for WUS in our study.

Our analysis of the AP2 mutant lines agrees with the existing hypothesis that AP2 promotes WUS expression, although its role in the expansion of the WUS domain remains unclear. The promotion of WUS expression by AP2 has been hypothesised to be either by direct promotion or through inhibiting CLV3's repression on WUS(Würschum *et al.*, 2006). An interesting feature that we observed is that AP2 mutants do not show differences from wild-type in their CLV3 expression domains. This may be due to the fact that the effect of WUS on CLV3 follows after a delay, which the time frame of our study might not have been able to capture.

4.3 Future Directions and Outlook

Our study has established a quantitative description of the dynamics of WUS and CLV3 during floral transition. Next steps to further our understanding of the system could involve explorations in multiple directions under the framework of computational morphodynamics.

4.3.1 Experimental Studies

We analysed the expression profiles of two genes in the wild-type and two mutant lines to study stem-cell homeostasis at the SAM. Future studies could look at more gene expression patterns in the wild-type and in more mutant backgrounds affecting the floral transition. One step springing directly from our study would be to analyse marker lines of AP2 and perform the same analysis as we have done here. Such an exploration would help elucidate more clearly the role of AP2 in stem-cell homeostasis. Another possible direction is to study where the WUS protein localises using translational fusions. Such a study would be aided by the image analysis pipeline that we have developed.

4.3.2 Modelling Studies

This study has provided a cell resolution data to assess the WUS-CLV3 feedback loop model and possible hypotheses for the expansion of the WUS domain during floral transition. Testing out these hypotheses necessitate the exercise of computational modelling of the system. Existing models of WUS and CLV3 do not account for their temporal dynamics. The scaling behaviour of expression domains with meristem size also seem to be prime ground for modelling studies. The floral transition is a period of extensive cell growth and division, and models incorporating gene regulatory network dynamics with cellular growth and division would prove to be stronger tools for studying this particular system.

References

Bailoni A, Pape C, Hütsch N, Wolf S, Beier T, Kreshuk A, Hamprecht FA (2022). GASP, a generalized framework for agglomerative clustering of signed graphs and its application to Instance Segmentation ArXiv:1906.11713 [cs].

Barton MK (2010). Twenty years on: The inner workings of the shoot apical meristem, a developmental dynamo. Developmental Biology 341(1), 95–113.

Bowman JL, Eshed Y (2000). Formation and maintenance of the shoot apical meristem. Trends in Plant Science 5(3), 110–115.

Brand U, Fletcher JC, Hobe M, Meyerowitz EM, Simon R (2000). Dependence of stem cell fate in arabidopsis on a feedback loop regulated by CLV3 activity 289(5479), 617–619.

Brand U, Grünewald M, Hobe M, Simon R (2002). Regulation of CLV3 Expression by Two Homeobox Genes in Arabidopsis. Plant Physiology 129(2), 565–575.

Busch W, Miotk A, Ariel FD, Zhao Z, Forner J, Daum G, Suzaki T, Schuster C, Schultheiss SJ, Leibfried A, Haubeiß S, Ha N, Chan RL, Lohmann JU (2010). Transcriptional Control of a Plant Stem Cell Niche. Developmental Cell 18(5), 841–853.

Bäurle I, Dean C (2006). The timing of developmental transitions in plants. Cell 125(4).

Clark S, Running M, Meyerowitz E (1995). CLAVATA3 is a specific regulator of shoot and floral meristem development affecting the same processes as CLAVATA1. Development 121, 2057–2067.

Clark SE, Running MP, Meyerowitz EM (1993). CLAVATA1, a regulator of meristem and flower development in Arabidopsis. Development (Cambridge, England) 119(2), 397–418.

Conti L (2017). Hormonal control of the floral transition: Can one catch them all? Developmental Biology 430(2), 288–301.

Daum G, Medzihradszky A, Suzaki T, Lohmann J (2014). A mechanistic framework for noncell autonomous stem cell induction in Arabidopsis. Proceedings of the National Academy of Sciences of the United States of America 111.

Ester M, Kriegel HP, Sander J, Xu X (1996). A density-based algorithm for discovering clusters in large spatial databases with noise. proceedings of the second international conference on knowledge discovery and data mining .

Fletcher JC, Brand U, Running MP, Simon R, Meyerowitz EM (1999). Signaling of cell fate decisions by CLAVATA3 in Arabidopsis shoot meristems. Science (New York, NY) 283(5409), 1911–1914.

Formosa-Jordan P, Teles J, Jönsson H (2022). Single-cell approaches for understanding morphogenesis using computational morphodynamics. In RJ Morris, editor, Mathematical Modelling in Plant Biology, 87–106.

Fuchs M, Lohmann JU (2020). Aiming for the top: non-cell autonomous control of shoot stem cells in Arabidopsis. Journal of Plant Research 133(3), 297–309.

Geier F, Lohmann JU, Gerstung M, Maier AT, Timmer J, Fleck C (2008). A quantitative and dynamic model for plant stem cell regulation. PloS one 3(10).

Gruel J, Deichmann J, Landrein B, Hitchcock T, Jönsson H (2018). The interaction of transcription factors controls the spatial layout of plant aerial stem cell niches. npj Systems Biology and Applications 4(1).

Gruel J, Landrein B, Tarr P, Schuster C, Refahi Y, Sampathkumar A, Hamant O, Meyerowitz EM, Jönsson H (2016). An epidermis-driven mechanism positions and scales stem cell niches in plants. Science Advances 2(1), e1500989.

Hohm T, Zitzler E, Simon R (2010). A Dynamic Model for Stem Cell Homeostasis and Patterning in Arabidopsis Meristems. PLOS ONE 5(2), e9189.

Jönsson H, Heisler M, Reddy GV, Agrawal V, Gor V, Shapiro BE, Mjolsness E, Meyerowitz EM (2005). Modeling the organization of the WUSCHEL expression domain in the shoot apical meristem 21, i232–i240.

Kinoshita A, Vayssières A, Richter R, Sang Q, Roggen A, van Driel AD, Smith RS, Coupland G (2020). Regulation of shoot meristem shape by photoperiodic signaling and phytohormones during floral induction of Arabidopsis. eLife 9, e60661.

Laufs P, Grandjean O, Jonak C, Kiêu K, Traas J (1998). Cellular parameters of the shoot apical meristem in Arabidopsis. The Plant Cell 10(8), 1375–1390.

Laux T, Mayer KF, Berger J, Jürgens G (1996). The WUSCHEL gene is required for shoot and floral meristem integrity in Arabidopsis. Development (Cambridge, England) 122(1), 87–96.

Long JA, Moan EI, Medford JI, Barton MK (1996). A member of the KNOTTED class of homeodomain proteins encoded by the STM gene of Arabidopsis. Nature 379(6560), 66–69.

Lopes FL, Galvan-Ampudia C, Landrein B (2021). WUSCHEL in the shoot apical meristem: old player, new tricks 72(5), 1527–1535.

Mayer KF, Schoof H, Haecker A, Lenhard M, Jürgens G, Laux T (1998). Role of WUSCHEL in Regulating Stem Cell Fate in the Arabidopsis Shoot Meristem. Cell 95(6), 805–815.

Okamuro JK, Caster B, Villarroel R, Montagu MV, Jofuku KD (1997). The AP2 domain of APETALA2 defines a large new family of DNA binding proteins in Arabidopsis. Proceedings of the National Academy of Sciences of the United States of America 94(13), 7076.

Pfeiffer A, Janocha D, Dong Y, Medzihradszky A, Schöne S, Daum G, Suzaki T, Forner J, Langenecker T, Rempel E, Schmid M, Wirtz M, Hell R, Lohmann JU (2016). Integration of light and metabolic signals for stem cell activation at the shoot apical meristem. eLife 5, e17023.

Poethig RS (1987). Clonal Analysis of Cell Lineage Patterns in Plant Development. American Journal of Botany 74(4).

Remadevi Vijayan A (2022). A digital quantitative and spatial reference atlas from microscopic 3d images of ovules in arabidopsis thaliana 172.

Sang Q, Vayssières A, Ó'Maoiléidigh DS, Yang X, Vincent C, Bertran Garcia de Olalla E, Cerise M, Franzen R, Coupland G (2022). MicroRNA172 controls inflorescence meristem size through regulation of APETALA2 in Arabidopsis. New Phytologist 235(1), 356–371.

Schoof H, Lenhard M, Haecker A, Mayer KFX, Jürgens G, Laux T (2000). The Stem Cell Population of Arabidopsis Shoot Meristems Is Maintained by a Regulatory Loop between the CLAVATA and WUSCHEL Genes. Cell 100(6), 635–644.

Stringer C, Wang T, Michaelos M, Pachitariu M (2021). Cellpose: a generalist algorithm for cellular segmentation 18(1), 100–106.

Su Y, Zhou C, Li Y, Yu Y, Tang L, Zhang W, Yao W, Huang R, Laux T, Zhang X (2020). Integration of pluripotency pathways regulates stem cell maintenance in the Arabidopsis shoot meristem. Proceedings of the National Academy of Sciences 117, 202015248.

Wolny A, Cerrone L, Vijayan A, Tofanelli R, Barro AV, Louveaux M, Wenzl C, Strauss S, Wilson-Sánchez D, Lymbouridou R, Steigleder SS, Pape C, Bailoni A, Duran-Nebreda S, Bassel GW, Lohmann JU, Tsiantis M, Hamprecht FA, Schneitz K, Maizel A, Kreshuk A (2020). Accurate and versatile 3d segmentation of plant tissues at cellular resolution 9, e57613.

Würschum T, Groß-Hardt R, Laux T (2006). APETALA2 regulates the stem cell niche in the arabidopsis shoot meristem The Plant Cell 18(2), 295–307.

Yadav RK, Perales M, Gruel J, Girke T, Jönsson H, Reddy GV (2011). WUSCHEL protein movement mediates stem cell homeostasis in the Arabidopsis shoot apex. Genes & Development 25(19), 2025–2030.

Yadav RK, Perales M, Gruel J, Ohno C, Heisler M, Girke T, Jönsson H, Reddy GV (2013). Plant stem cell maintenance involves direct transcriptional repression of differentiation program. Molecular Systems Biology 9, 654.

Yant L, Mathieu J, Dinh TT, Ott F, Lanz C, Wollmann H, Chen X, Schmid M (2010). Orchestration of the Floral Transition and Floral Development in Arabidopsis by the Bifunctional Transcription Factor APETALA2. The Plant Cell 22(7), 2156–2170.

Zhou Y, Liu X, Engstrom EM, Nimchuk ZL, Pruneda-Paz JL, Tarr PT, Yan A, Kay SA, Meyerowitz EM (2015). Control of plant stem cell function by conserved interacting transcriptional regulators. Nature 517(7534), 377–380.

Zhou Y, Yan A, Han H, Li T, Geng Y, Liu X, Meyerowitz EM (2018). HAIRY MERISTEM with WUSCHEL confines CLAVATA3 expression to the outer apical meristem layers. Science 361(6401), 502–506.

Ó'Maoiléidigh DS, D van Driel A, Singh A (2021). Systematic analyses of the MIR172 family members of Arabidopsis define their distinct roles in regulation of APETALA2 during floral transition | PLOS Biology .